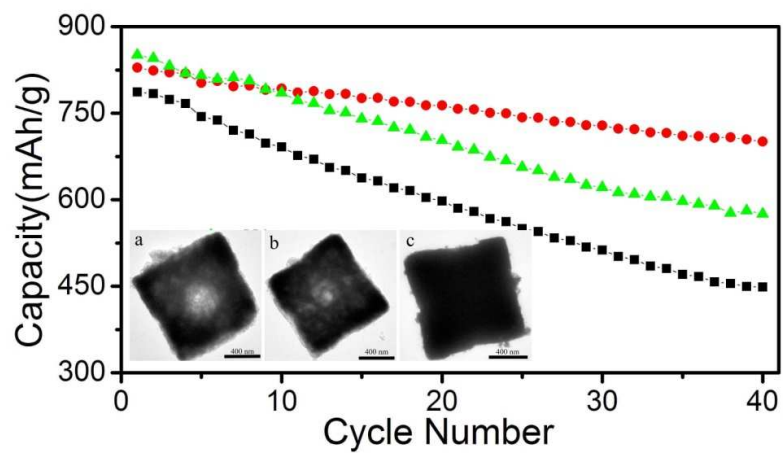




Porous SnO₂ nanocubes with controllable pore volume and their Li storage performance

Journal:	<i>RSC Advances</i>
Manuscript ID:	RA-ART-01-2014-000362.R1
Article Type:	Paper
Date Submitted by the Author:	17-Feb-2014
Complete List of Authors:	Weij, Wei; beijing university of Aeronautics and Astronautics, Gao, Sen; BEIJING UNIVERSITY OF AERONAUTICS & ASTRONAUTICS, Chemistry Wu, Yongmin; Tsinghua Univ., Chem. Yang, Zhao; BEIJING UNIVERSITY OF AERONAUTICS & ASTRONAUTICS, Chemistry Chen, Chang; BEIJING UNIVERSITY OF AERONAUTICS & ASTRONAUTICS, Chemistry Guo, Lin; BEIJING UNIVERSITY OF AERONAUTICS & ASTRONAUTICS, Chemistry Li, Jinghong; Tsinghua Univ, Chemistry



SnO₂ nanocubes with controllable pore volume show best Li storage performance.

Cite this: DOI: 10.1039/c0xx00000x

ARTICLE TYPE

www.rsc.org/xxxxxx

Porous SnO₂ nanocubes with controllable pore volume and their Li storage performance

Wei Wei^a, Sen Gao^a, Zhao Yang^a, Yongmin Wu^b, Chang Chen^a, Lin Guo^{a*} and Jinghong Li^{b*}

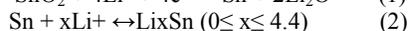
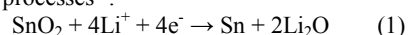
Received (in XXX, XXX) Xth XXXXXXXXX 20XX, Accepted Xth XXXXXXXXX 20XX

DOI: 10.1039/b000000x

In order to optimize the cycling performance of porous SnO₂ nanomaterials, we designed porous SnO₂ nanocubes with controllable pore volume via two strategies by using CaSn(OH)₆ microcubes as templates. The formation mechanism, morphology and microstructure of the as-prepared products were investigated by various techniques, including powder X-ray diffraction (XRD), scanning electron microscopy (SEM), transmission electron microscopy (TEM), high-resolution TEM and N₂ absorption-desorption analysis. The Li storage performance of the porous SnO₂ nanocubes as anode materials for Li ion batteries was also studied. Results show that SnO₂ nanocubes with an appropriate pore volume exhibited best Li storage performance. For example, SnO₂ nanocubes prepared by the calcination-dissolution-dissolution strategy with pore volume of 0.257 cc/g exhibited capacity retention up to 85.7% after 40 cycles, while lower or higher than this value resulted in rapid capacity depreciation.

1. Introduction

The development of hybrid and electric vehicles has created the need to realize high energy density and long-lasting Li-ion batteries (LiBs). As a potential candidate for Li-ion battery anode material, SnO₂ has been extensively studied as an alternate anode material to the commercial graphite because of its much higher theoretical capacity (782 mAh·g⁻¹ compared with 372 mAh·g⁻¹). It is believed that SnO₂ reacts with lithium in the following two step processes¹:



The conversion reaction in Eq. (1) is usually considered as electrochemically irreversible with no capacity contribution. The alloying/de-alloying reaction (2) is thought to be highly reversible, providing a theoretical specific capacity of 782 mAh/g for SnO₂. However, the volume change is about 240% when Sn reacts with Li to form Li_{4.4}Sn². The huge volume variation leads to fatigue failure and disintegration of the active material, and causes a so-called pulverization problem, which blocks the electrical contact pathways between adjacent particles and results in rapid capacity fading.

To overcome the problems related with SnO₂ anodes for LiBs, several strategies have been developed during the past decades³⁻²³. These strategies can be divided into two categories as follows. The first strategy is to prepare SnO₂ composite electrodes with other efficient materials, such as carbon³⁻⁵, carbon nanotubes^{6,7}, graphene⁸⁻¹², conductive polymers¹³, and so on¹⁴. The second strategy is to prepare SnO₂ nanomaterials. Various morphologies of SnO₂ nanomaterials, such as porous/hollow structures¹⁵⁻¹⁹, nanosheets²⁰, nanorods/nanowires^{21,22} and thin films²³ etc., can be used for this purpose. Particularly, porous SnO₂ nanomaterials exhibit fascinating cycling performance because their local pores could accommodate the large volume change during cycling, thus delaying capacity fades. To further improve the cycling performance of porous/hollow metal oxide anodes, designing

them with an appropriate pore volume may be a possible way²⁴. It is speculated that porous/hollow metal oxide anodes with appropriate pore volume could correctly accommodate the volume expansion and keep their structure stable during charge/discharge cycles. In order to verify this idea, we designed SnO₂ nanocubes with controllable pore volume by using CaSn(OH)₆ microcubes as sacrificial template. The feature of our work is, SnO₂ nanocubes with controllable pore volumes can be prepared by two strategies using the same template. Electrochemical tests indicate that, porous SnO₂ nanocubes anodes with appropriate pore volume show best cycling performance.

2. Experiment

2.1 Preparation of materials

CaSn(OH)₆ microcubes were prepared according to the previous literatures^{25,26}.

Table 1 experimental parameters of the two methods prepared SnO₂ nanocubes.

Methods	Calcinations	16 M HNO ₃	0.5 M HCl
		treatment (h)	treatment (h)
CDD	3 h at 700 °C	8/10/12/14/16	24
CD	40/60/80 min at 350 °C	0	10

For the calcination-dissolution-dissolution (CDD) strategy, 5 parallel CaSn(OH)₆ samples were first calcined at 700 °C for 3 h followed by immersing in 20 mL of 16 M HNO₃ for 8, 10, 12, 14, 16 h, respectively. The products were collected by centrifugation, washed several times by deionized water, dried at 80 °C. Next, the products were poured into 50 mL HCl solution (0.5 M) for 24

h. After washing several times, porous SnO₂ nanocubes with different pore volumes were obtained.

For calcination-dissolution (CD) strategy, 3 parallel CaSn(OH)₆ samples were calcined at 350 °C for 40, 60 and 80 min, respectively. The calcined products were then immersed in 50 mL 0.5 M HCl for 10 h, porous SnO₂ nanocubes with different pore volumes were obtained after washing and drying.

Table 1 shows the experimental parameter of the SnO₂ nanocube samples.

2.2 Characterizations

The X-ray diffraction (XRD) spectra of the samples were recorded by a Rigaku Dmax 2200 X-ray diffractometer with Cu-K α radiation (λ=1.5416 Å). The morphologies of the samples were obtained using a scanning electron microscope (SEM, Hitachi S-4800, 5.0 KV). Transmission electron microscopy (TEM) and high-resolution TEM (HRTEM) investigations accompany with SAED (selected area electron diffraction) were carried out by a JEOL JEM-2100F microscope with an accelerate voltage of 20 KV. Specific surface areas of the samples were measured at 77 K by Brunauer-Emmett-Teller (BET) nitrogen adsorption-desorption (NOVA 2200e, Quantachrome, USA.), pore volumes were calculated by Barrett-Joyner-Halenda (BJH) method.

2.3 Electrochemical performance

The electrochemical reactions of samples with lithium were investigated using a simple two-electrode cell. A N-methyl pyrrolidinone (NMP) slurry consisting of 80 wt.% of the active material powder, 10 wt.% of carbon black and 10 wt.% of PVDF was uniformly coated on a copper disk of 14 mm in diameter. The disk electrodes were dried overnight at 80 °C followed by compression at 1.0×10⁶ Pa. The 2016 coin cells were assembled in an Ar-filled glove box using polypropylene (PP) micro-porous film as the separator. A solution of 1 M LiPF₆ in ethylene carbonate (EC)/dimethyl carbonate (DMC) (1:1, v/v) was used as electrolyte and metallic lithium foil as counter electrode. The charged and discharged tests were performed galvanostatically on a CT2001A Land battery testing systems. The cells were charged and discharged at various current and a constant temperature of 25 °C in the voltage range of 0.005 ~ 1.5 V. The electrochemical impedance measurements were performed on CHI660D electrochemical workstation at an AC voltage of 5 mV amplitude in the 100 kHz to 0.01 Hz.

3. Results and discussion

3.1 CDD strategy

Figure S1(Electronic Supplementary Information) shows the SEM image of the as-prepared CaSn(OH)₆. It can be observed that CaSn(OH)₆ is of perfect cubic morphology with a diameter of 0.8 ~ 1 μm. For the CDD strategy, CaSn(OH)₆ microcubes were initially converted to CaSnO₃ microcubes by calcinations. Subsequently, the CaSnO₃ microcubes were immersed in HNO₃ at varying duration of time to form SnO₂/CaSnO₃ mixture; lastly, porous SnO₂ nanocubes were obtained after the removal of CaSnO₃ by HCl. The HNO₃ treatment time of the CaSnO₃ microcubes has a great influence on the pore volume of the SnO₂ nanocubes, from which, the pore volume of the SnO₂ nanocubes can be controlled. Herein, we noted SnO₂ nanocubes obtained after 8, 10, 12, 14 and 16 h HNO₃ treatment as S8, S10, S12, S14 and S16, respectively.

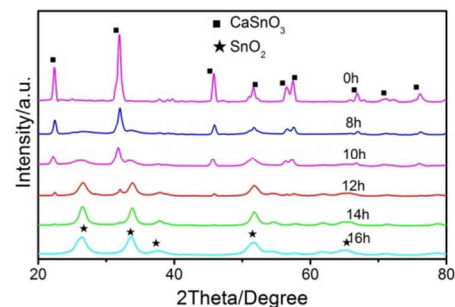


Figure 1. (a) XRD patterns of CaSnO₃ samples with different HNO₃ treatment time.

The XRD patterns of CaSnO₃ and CaSnO₃/SnO₂ mixture with different HNO₃ treatment time are shown in Figure 1. For CaSnO₃, all the reflection peaks can be indexed to orthorhombic CaSnO₃ with a perovskite structure (JCPDS card No. 31-0312), which indicates that a pure phase CaSnO₃ is obtained. For these CaSnO₃/SnO₂ mixtures, the CaSnO₃ peaks shrink and the SnO₂ peaks become sharp gradually with prolong HNO₃ treatment time. When the HNO₃ treatment time reaches 16h, all the diffraction peaks well match to rutile structured SnO₂ (JCPDS card No. 41-1445), which indicates the CaSnO₃ has been completely transformed to SnO₂. It is clear that more SnO₂ component can be obtained with longer HNO₃ treatment time. Figure S2 (Electronic Supplementary Information) shows the XRD patterns of S8, S12 and S16. All the diffraction peaks are related to rutile structured SnO₂, and no signals of CaSnO₃ or byproducts are detected for S8 and S12, which imply that the CaSnO₃ component in the mixture was completely removed by diluted HCl. The broad XRD peaks of S8, S12 and S16 suggest the small primary particles of the as-synthesized SnO₂. Based on the Scherrer equation, the average particle sizes of S8, S12 and S16 are calculated to be 7.2 nm, 7.4 nm and 7.1 nm, respectively. The average particle sizes of the three samples are almost the same, and it may be due to the same formation mechanisms (see Eq. 3 and Eq. 4). Based on the XRD analysis, possible formation mechanisms of the SnO₂ nanocubes are speculated as following:

$$\text{CaSnO}_3(\text{s}) + 2\text{xHNO}_3(\text{aq}, 16\text{M}) \rightarrow (1-\text{x}) \text{CaSnO}_3/\text{xSnO}_2(\text{s}) + \text{xCa}^{2+}(\text{aq}) + 2\text{xNO}_3^{2-}(\text{aq}) + \text{xH}_2\text{O} \quad (0\text{h} < \text{t} < 16\text{h}, 0 < \text{x} < 1) \quad (3)$$

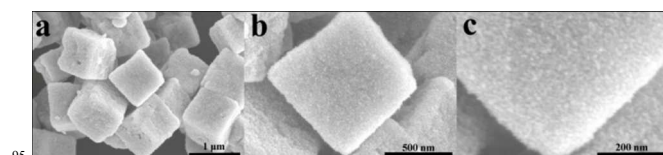
$$(1-\text{x}) \text{CaSnO}_3/\text{xSnO}_2(\text{s}) + 6(1-\text{x})\text{HCl}(\text{aq}, 0.5\text{M}) \rightarrow \text{xSnO}_2(\text{s}) + (1-\text{x}) \text{Ca}^{2+}(\text{aq}) + (1-\text{x}) \text{Sn}^{4+}(\text{aq}) + 6(1-\text{x}) \text{Cl}^{-}(\text{aq}) + 3(1-\text{x})\text{H}_2\text{O} \quad (0\text{h} < \text{t} < 16\text{h}, 0 < \text{x} < 1) \quad (4)$$


Figure 2. SEM images of (a) S10, (b) a single nanocube of S10 and (c) its partial magnified image

Figure 2a is the typical SEM image of S10, it can be seen that the SnO₂ products are of cubic shape with a uniform particle size in the range of 0.8 ~ 1 μm. Figure 2b and c show a single SnO₂ cube and its partial magnified image. From Figure 2b, it can be found that the surface of the SnO₂ nanocube is quite rough. From Figure 2c, a magnified part of Figure 2b, it can be clearly seen that the SnO₂ nanocube is consisted of small SnO₂ nanoparticles.

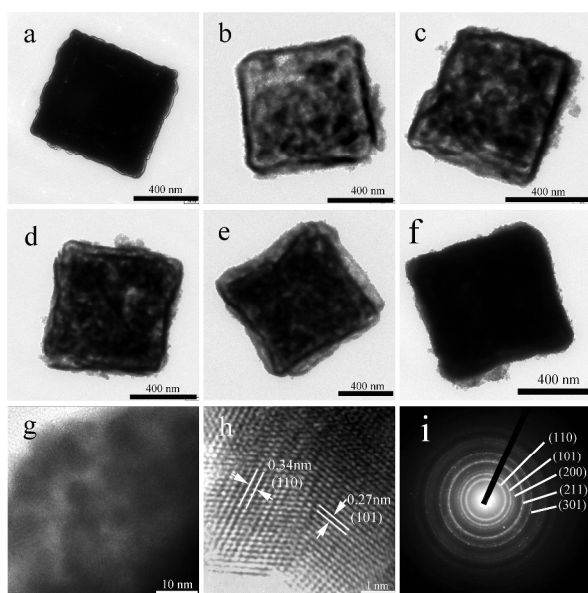


Figure 3. Typical TEM images of CaSnO_3 and SnO_2 nanocubes: a) CaSnO_3 , b) S8, c) S10, d) S12, e) S14 and f) S16; g) the magnified TEM image of S8, h) the HRTEM image of S8, i) SAED patterns of S8.

TEM and HRTEM accompanied with selected area electron diffraction (SAED) were performed to further characterize the morphologies and microstructures of the samples. From Figure 3a, it can be observed that the CaSnO_3 sample is of cubic shape. Figure 3b, c, d, e and f, clearly shows that after HNO_3 and HCl treatments, respectively, all the SnO_2 nanocubes still retained the original cubic morphology of their precursors. In addition, the SnO_2 nanocubes have similar particle size compared with their precursors. Only dark cubic shape product can be observed in Figure 3a, which implies the solid nature of the CaSnO_3 cubes. In Figure 3b, the obvious brightness contrast of the SnO_2 nanocube reveals large pore volume inside. From Figure 3b to Figure 3e (S8 to S14), the brightness contrast of the SnO_2 nanocubes becomes weaker, indicating the gradual loss of pore volume of these nanocubes. For S16 (Figure 3f), the similar TEM image as CaSnO_3 indicates the solid inner structure of the sample. Figure 3g is the high magnified TEM image of an edge of S8. The average size of SnO_2 nanoparticles is about 7 nm, which perfectly matches with the above XRD analysis. In addition, many mesopores with mean diameter of 4 nm can be seen. According to the above TEM analysis, we can confirm that two kinds of pores have been produced in S8, S10, S12 and S14: the first kind is the mesopores with a diameter of ~ 4 nm probably caused by the removal process of Ca^{2+} and H_2O (Eq. 3), and the second is large pore with a diameter of several tens to hundred nanometer probably caused by the removal process of CaSnO_3 (Eq. 4). Only mesopores exist in S16. This conclusion will be further determined by the BET analysis in the later section. Figure 3h is the HRTEM image of S8. Clear lattice fringes of small SnO_2 nanocrystals can be observed, and interplanar spacing were measured to be 0.34 nm and 0.27 nm, consistent with the d values of the (110) and (101) planes of the tetragonal rutile SnO_2 , respectively. The diffraction rings in the SAED patterns recorded at the edges of the cube (Figure 3i) indicate their polycrystalline

nature, and the rings from inside to outside can be assigned to (110), (101), (200), (211) and (301) planes of rutile SnO_2 .

By comparative experiments, we found that HNO_3 concentration and treatment time are two important factors in determining the final morphology of the products. (1) The concentrated HNO_3 plays a key role in maintaining the cubic structure of the final products. When HNO_3 was diluted, with the reaction time of 16 h, only irregular SnO_2 particles can be obtained (Electronic Supplementary Information Fig. S3). It is speculated that the formation of SnO_2 was an *in situ* process in the concentrated HNO_3 due to its strong oxidative ability. Thus, the resulted SnO_2 can retain the cubic morphology of its precursor. When the concentrated HNO_3 was diluted, the oxidative ability decreased, Sn^{4+} ions were released to the diluted HNO_3 solution and formed SnO_2 nanoparticles. (2) Sufficient HNO_3 treatment time of the CaSnO_3 precursor is necessary in keeping the regular morphology of SnO_2 nanocubes. When the HNO_3 treatment time was reduced to 6 h, it can be seen that SnO_2 nanoparticles and some broken SnO_2 nanocubes co-exist in the visual field (Electronic Supplementary Information Fig. S4). According to XRD analysis, the SnO_2 component should be much less than CaSnO_3 in the mixture. In the removal process of the CaSnO_3 component, the cubes collapsed, as the SnO_2 component were not enough to keep the original cubic morphology. Therefore, in order to obtain regular SnO_2 nanocubes, the HNO_3 pretreatment time is required beyond 8 h.

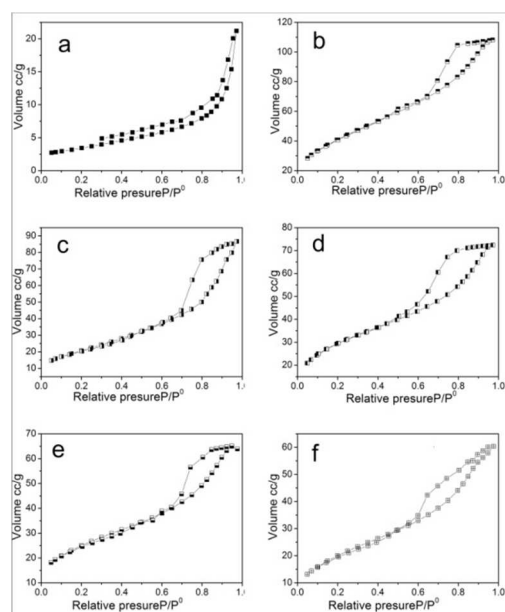


Figure 4. Nitrogen adsorption and desorption isotherms of a) CaSnO_3 , b) S8, c) S10, d) S12, e) S14 and f) S16

The porous structural feature of these SnO_2 nanocubes is confirmed by N_2 sorption measurements. Figure 4 shows the adsorption-desorption isotherms of the SnO_2 nanocube samples. Except CaSnO_3 and S16, all of the samples exhibit a type IV N_2 adsorption-desorption isotherm with a type H2 hysteresis loop. H2 hysteresis loop is a characteristic of wide pore size distribution when irrespective of pore shape and pore connectivity²⁷. The adsorption-desorption isotherm of CaSnO_3 shows that the sample is non-porous. S16 shows a type IV N_2 adsorption-desorption isotherm with a type H3 hysteresis loop, indicating mesoporous structure²⁸. Pore volume data (Electronic Supplementary Information Table 1) show that by using this

strategy the pore volume of the SnO₂ nanocubes can be controlled at 0.332 ~ 0.092 cc/g.

3.2 CD strategy

The CD strategy is relatively simple. Firstly, CaSn(OH)₆ microcubes were partially converted to CaO/SnO₂ by calcination at 350 °C within 80 min and formed CaSn(OH)₆/CaO/SnO₂ mixtures; then the CaSn(OH)₆/CaO components in the mixture were dissolved by diluted HCl and remained porous SnO₂ nanocubes. The pore volume of the SnO₂ nanocubes can be controlled by altering the calcination time. Compared with the CDD strategy, this strategy needs lower calcination temperature, less acid treatment step and time. Herein, we note the porous SnO₂ nanocubes obtained by 40, 60 and 80 min calcination as M1, M2 and M3.

Figure 5a shows the XRD patterns of CaSn(OH)₆, which matches well with JCPDS card No. 74-1823. It is reported that at the temperature range of 250 ~ 500 °C, CaSn(OH)₆ decomposes and forms CaO/SnO₂ composite²⁹. Figure 5d shows the XRD patterns of CaSn(OH)₆ calcined at 350 °C for 80 min, two broad peaks located at around 35° and 55° can be found, which are same as the reported results and corresponding to CaO/SnO₂ mixture²⁹. It is clear that CaSn(OH)₆ were completely decomposed after 80 min calcination at 350 °C. While the calcination time was lower than 80 min, CaSn(OH)₆ did not decompose completely and formed CaO/SnO₂/CaSn(OH)₆ composite. Figure 5b and c show the XRD patterns of CaSn(OH)₆ calcined at 350 °C for 40 and 60 min, respectively. It can be found that the final products are consisted of CaO/SnO₂/CaSn(OH)₆. Furthermore, the peaks intensity of CaO/SnO₂ increased while CaSn(OH)₆ shrink with prolong calcination time.

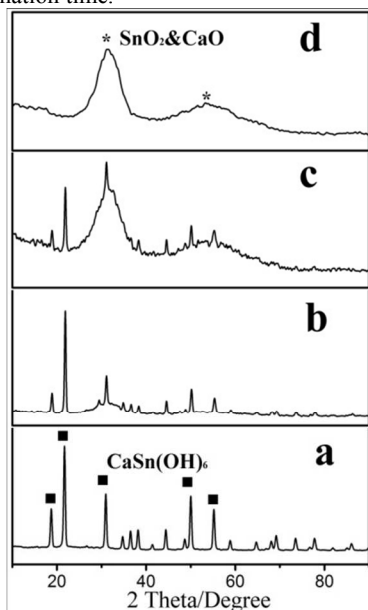


Figure 5. XRD patterns of CaSn(OH)₆ samples with different calcination time at the temperature of 350 °C: (a), (b), (c) and (d) corresponding 0, 40, 60 and 80 min.

Figure S5 (Electronic Supplementary Information) is the XRD pattern of M2, the diffraction peaks can be indexed to rutile structured SnO₂ with JCPDS card No. 41-1445. The pure phase SnO₂ obtained suggests that after diluted HCl treatment, the CaO/CaSn(OH)₆ components were completely removed. So the formation mechanism of the SnO₂ products can be written as follows:

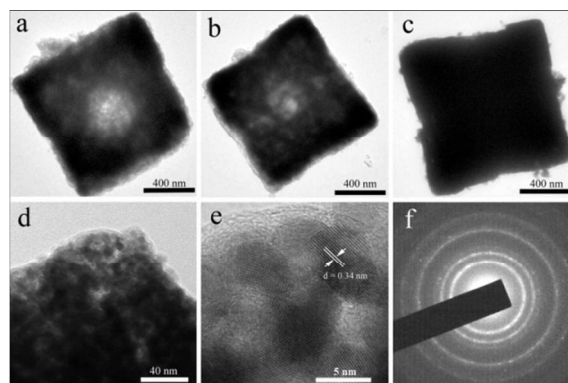
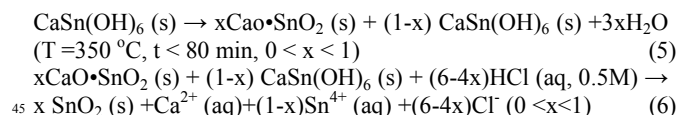


Figure 6. Typical TEM images of SnO₂ nanocubes: a) M1, b) M2 and c) M3; d) the magnified TEM image of M1, e) the HRTEM image of M1 and f) SAED patterns of M1.

Figure 6a, b and c show the typical TEM image of M1, M2 and M3, respectively. It can be seen that SnO₂ products prepared by this strategy can also maintain their precursor's cubic shape. From the brightness contrast, we can see that the pore volume gradually reduced from M1 to M3. The large hollows which exists in M1 and M2 could be speculated to have been caused by the dissolution of CaSn(OH)₆. Figure 6d is the high magnification TEM image of M1, from which it can be seen that the SnO₂ nanocube is consisted of SnO₂ nanoparticles with mesopores existence. The mesopores are speculated to be caused by the process of CaO dissolution. Figure 6e is the HRTEM image of M1. The interplanar spacing of 0.34 nm matches the (110) plane of rutile structured SnO₂. The primary particle size of the SnO₂ nanocubes is measured to be ~ 7 nm, which is comparable to that prepared by the CDD strategy. Furthermore, the mesopore diameter of 3 ~ 4 nm can be estimated from Figure 6e. Figure 6f, the SAED patterns of M1, which has the same appearance with Figure 3i, indicates the polycrystalline nature of the as-prepared SnO₂ nanocubes.

By using this strategy, the pore volume of the SnO₂ nanocubes can be controlled at the range of 0.1101 ~ 0.2932 cc/g (Electronic Supplementary Information Table 2).

3.3 Li storage performance

Firstly, we try to find the appropriate pore volume of the CDD strategy prepared SnO₂ nanocube anodes. The cycling performance of these electrodes was evaluated, as shown in Figure 7a. After 40 cycles, the charge capacity retentions for S8, S10, S12, S14 and S16 electrodes are 79.3%, 85.7%, 77.8%, 65.0% and 57.7%, respectively. Obviously, S10 has the highest capacity retention. This implies that SnO₂ nanocubes with a pore volume 0.257cc/g can effectively buffer the volume change and keep structural stability during cycling. In order to confirm our speculation, direct evidences are supplied by disassembling some of the cells to observe the morphology changes of the SnO₂ nanocubes. Figure S6a, b and c (Electronic Supplementary Information) corresponding to the TEM images of S8, S10 and S14 at the end of 10th charge/discharge cycle, respectively. It can be observed that after 10 cycles, S10 can still keep their original cubic morphology with less damage. For S8, some broken

nanocubes can be found, which were probably caused by their poorer structural stability compared with S10. Almost all the nanocubes of S14 were broken, indicating the pore volume of the sample was not sufficient to buffer the volume change during cycling.

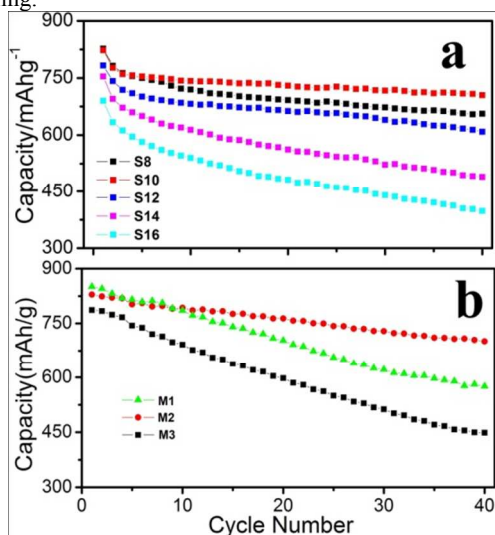


Figure 7. Capacity retention of (a) CDD and (b) CD strategy prepared electrodes (0.005 ~ 1.5 V, 0.2 C).

Figure 7b shows the cycling performance of SnO₂ nanocubes prepared by CD strategy with the same charge-discharge conditions. The charge capacity retentions at the end of 40 cycles for M1, M2 and M3 are 67.6%, 84.4% and 57.1%, respectively. Electrode M2 with the pore volume 0.244 cc/g exhibited best cycling performance. It can be found that the appropriate pore volume values of the porous SnO₂ nanocubes obtained by the two strategies are very close. This is because the SnO₂ nanocubes prepared by the above strategies have the same morphology and particle size.

4. Conclusions

In order to optimize the cycling performance of porous SnO₂ nanomaterials anodes, we successfully designed porous SnO₂ nanocubes with controllable pore volumes by using the template of CaSn(OH)₆ microcubes via two strategies. For the CDD strategy, the pore volume of 0.332 ~ 0.092 cc/g can be accurately controlled by simply adjusting the HNO₃ treatment time of CaSnO₃, while for the CD strategy the pore volume of 0.1101 ~ 0.2932 cc/g can be controlled by altering the calcination time of CaSn(OH)₆. Electrochemical tests showed that porous SnO₂ nanocubes with an appropriate pore volume have the best cycling performance. For the CDD strategy, SnO₂ nanocubes with a pore volume 0.257cc/g shows the best cycling performance, their capacity retention reach up to 85.7% after 40 cycles; while for the CD strategy, SnO₂ nanocubes with the pore volume 0.244 cc/g exhibited best cycling performance, the capacity retention of 84.4% can be reached after 40 cycles. Except the more complex synthesis method of CDD strategy, the morphology, optimized pore volume and cycling performance for both strategies synthesized products are very close.

Acknowledgment. This work was financially supported by the National Basic Research Program of China (2010CB934700, 2013CB934004, 2011CB935704) and National Natural Science Foundation of China (11079002).

Notes and references

- ^a School of Chemistry and Environment, Beihang University, Beijing 100191, China E-mail: guolin@buaa.edu.cn
^b Department of Chemistry, Beijing Key Laboratory for Microanalytical Methods and Instruments, Tsinghua University, Beijing 100084, China; E-mail: jhli@mails.tsinghua.edu.cn
[†] Electronic Supplementary Information (ESI) available: [details of any supplementary information available should be included here]. See DOI: 10.1039/b000000x/
- I. A. Courtney and J. R. Dahn, *J. Electrochem. Soc.* 1997, **144**, 2045.
 - J. Huang, L. Zhong, C. Wang, J. P. Sullivan, W. Xu, L. Q. Zhang, S. X. Mao, N. S. Hudak, X. H. Liu, A. Subramanian, H. Fan, L. Qi, A. Kushima and J. Li. *Science* 2010, **330**, 1515.
 - R. Yang, W. Zhao, J. Zheng, X. Zhang and X. Li, *J. Phys. Chem.* 2010, **114**, 20727.
 - X. W. Lou, J. S. Chen, P. Chen and L. A. Archer, *Chem. Mater.* 2009, **21**, 2868.
 - X. Sun, J. Liu and Y. Li, *Chem. Mater.* 2006, **18**, 3486.
 - L. Zhang, L. Jiang, C. Chen, W. Li, W. Song and Y. Guo, *Chem. Mater.* 2010, **22**, 414.
 - Z. Wen, Q. Wang, Q. Zhang and J. Li, *Adv. Funct. Mater.* 2007, **17**, 2772.
 - D. Chen, L. Tang and J. Li, *Chem. Soc. Rev.* 2010, **39**, 3157.
 - J. Liang, W. Wei, D. Zhong, Q. Yang, L. Li and L. Guo, *ACS Appl. Mater. Interf.* 2012, **4**, 454.
 - W. Wang, Q. Hao, W. Lei, X. Xia and X. Wang, *RSC Adv.* 2012, **2**, 10268.
 - X. Zhou, Y. X. Yin, L. J. Wan and Y. G. Guo, *J. Mater. Chem.* 2012, **22**, 17456.
 - L. S. Zhang, L. Y. Jiang, H. J. Yan, W. D. Wang, W. Wang, W. G. Song, Y. G. Guo and L. J. Wan, *J. Mater. Chem.* 2010, **50**, 5462.
 - J. Zhang, S. Wang, M. Xu, Y. Wang, H. Xia, S. Zhang, X. Guo and S. Wu, *J. Phys. Chem. C* 2009, **113**, 1662.
 - C. Li, W. Wei, S. Fang, H. Wang, Y. Zhang, Y. Gui and R. Chen., *J. Power Sources* 2010, **195**, 2939.
 - R. D. Cakan, Y. Hu, M. Antonietti, J. Maier and M. M Titirici, *Chem. Mater.* 2008, **20**, 1227.
 - D. Deng and J. Y. Lee., *Chem. Mater.* 2008, **20**, 1841.
 - W. Wei, Z. Wang, Z. Liu, Y. Liu, L. He, D. Chen, A. Umar, L. Guo and J. Li, *J. Power Sources* 2013, **238**, 376.
 - Y. Wang, J. Y. Lee and H. C. Zeng, *Chem. Mater.* 2005, **17**, 3899.
 - Z. Wang, D. Luan, F. Y. C. Boey and X. W. Lou, *J. Am. Chem. Soc.* 2011, **133**, 4738.
 - C. Wang, Y. Zhou, M. Ge, X. Xu, Z. Zhang and J. Z. Jiang, *J. Am. Chem. Soc.* 2010, **132**, 46.
 - X. Ji, X. Huang, J. Liu, J. Jiang, X. Li, R. Ding, Y. Hu, F. Wu and Q. Li, *Nanoscale Res Lett* 2010, **5**, 649.
 - M. Park, Y. Kang, G. Wang, S. Dou and H. Liu, *Adv. Funct. Mater.* 2008, **18**, 455.
 - X. Wang, X. L. Wu, Y. G. Guo, Y. Zhong, X. Cao, Y. Ma and J. Yao, *Adv. Funct. Mater.* 2010, **20**, 1680.
 - X. L. Wu, Y. G. Guo and L. J. Wan, *Chem. Asian J.* 2013, **8**, 1948.
 - Z. Lu, J. Liu, Y. Tang and Y. Li., *Inorgan. Chem. Commun.* 2004, **7**, 731.
 - H. Cheng and Z. Lu., *Solid State Sciences.* 2008, **10**, 1042.
 - Toshihide Horikawa, D. D. Do and D. Nicholson, *Adv. Coll. Inter. Sci.* 2011, **169**, 40.
 - H. X. Yang, J. F. Qian, Z. X. Chen, Xin P. Ai, Y. L. Cao., *J. Phys. Chem. C.* 2007, **111**, 14067.
 - Y. Sharma, N. Sharma, G. V. Subba Rao and B. V. R. Chowdari, *Chem. Mater.* 2008, **20**, 6829.